Design Complex-Stroke Press Using Synchronous Motors

Dang Anh-Tuan and Nguyen Dinh-Ngoc *

Faculty of International Training, Thai Nguyen University of Technology, Thai Nguyen, Vietnam
Email: anhtuanck@tnut.edu.vn (D.A.T.)
*Correspondence: ngocnd.cenis@tnut.edu.vn (N.D.N.)

***Abstract*—Despite the flexibility in the stamping process with complex ram movement, commercial servo presses are still expensive for the affordable of medium or small enterprises. Moreover, since the movement of the ram can be precisely controlled, these systems also require high maintenance and even highly skilled workers to operate. This study proposes a design for multi-stroke forging machines, which combines a gear transmission and a 6-link mechanism to control the stroke for the ram. Experiments with several design parameter sets prove the possibility of modifying the complex movement of the rams only by changing the gear ratio and angular difference between diving shafts. Results obtained from the calculation also indicate the applicability of the proposed system in multi-stage forging and support the designing process to get complex strokes of the ram.**

***Keywords*—forging, complex-stroke press, kinematic analysis, stress relaxation**

I. Introduction

Metal forming is a traditional process that is still commonly used today. Among these machines, presses are classic type that allows for changing the shape of workpieces by continuously applying pressure. These machines can be divided into mechanical, hydraulic, or pneumatic presses.

Metal forming is a traditional process that is still commonly used today. Among these machines, presses are a classic type that allows for changing the shape of workpieces by continuously applying pressure. These machines can be divided into mechanical, hydraulic, or pneumatic presses. In addition to the design of presses, the mechanical properties of the processed materials are also important issues that need attention since they affect mold manufacturing and the capacity of the machines. The stress relaxation characteristic of materials is no exception in this issue. This thermomechanical phenomenon, which is a time-dependent parameter where stress decreases under constant strain by creating intervals between deformations, can convert elastic strain to plastic strain, allowing the material easily to deform and avoid crack defects during the process. Moreover, this characteristic also helps reduce the requirement of workpiece heating for the deformation procedure [1]. Hence, the need to use complex strokes for forging or pressing on complex surfaces is crucial. Although mechanical presses are high-speed machines that can operate up to thousands of shots per minute with high-energy efficiency stored in flywheels, they are inflexible because the motions of rams depend on the structure of the connecting parts, which cannot be changed easily.

While hydraulic and pneumatic presses can create flexible programmed trajectories, these devices are not as energy efficient as mechanical ones due to the lack of flywheels. To increase the flexibility of the machine, several methods have been proposed. For instance, Mukasheva and Japayev *et al.* [2] constructed a simulation model of a six-bar mechanical press on Maple to analyze the dynamic behavior of the system while applying the conservation of energy law. The results of the study showed that the proposed method not only can automate the design process but also highlights the importance of using computers to analyze the kinematic and dynamic features of complex flat lever mechanisms. In another study, Hsieh and Tsai [3] proposed a design for an Oldham coupling that transmits constant speed from the driving motor to a 6-link mechanism for precision deep drawing processes. Experimental results on the prototype structure demonstrated the applicability and reasonable accuracy of the mechanism with advantages of easy manufacture, low cost, ease of adjustment, and high precision. For the study of functionality and synthesis of the Stephenson II crank-slider mechanism, Tuleshov and Akhmetova *et al.* [4] proposed a new analytical method to obtain formulas for the extreme pressure angle based on the geometric parameters of the mechanism. The results of the study demonstrate the operational capabilities of the kinematic structure of the Stephenson II crank-slider mechanism when optimizing this type of press while ensuring the highest force transfer. To analyze the dynamic behavior of a six-bar mechanical press and evaluate the reaction on the joints as well as the driving moment, Mitsi and Tsiafis *et al.* [5] used an analytical approach combined with an iterative method and d'Alembert's principle. By conducting

Manuscript received March 2, 2023; revised April 27, 2023; accepted May 10, 2023.

doi: 10.18178/ijmerr.12.4.249-257

simulations using MATLAB software, the study suggests the possibility of optimizing the structure of the press while considering different constraints without the need to construct a physical model. By combing Watt II and Stephenson III mechanisms, Jo and Shim *et al.* [6] developed a six-bar slider-crank stamping machine. To determine the exact dimensions of all the links in the device based on the specified positions of the slider, the homotopy continuation method optimization was utilized. To improve the computation process, newly developed homotopy continuation methods were employed, resulting in a significant reduction in calculation time.

The development of servomotors has opened up new possibilities for programmable mechanical presses, allowing for more efficient and flexible operations. Several systems that use servo motors have been proposed, and advantageous techniques have been applied to the presses to make the control of ram movement easier. Soong [7] proposed a 6-link mechanism to construct a single Degree-Of-Freedom (DOF) mechanical press with a length-adjustable link. By using a servomotor with a specific speed diagram, the length of driver link can be programmed and adjusted, making the slider to move with designated motions. By combining servo motors and synchronous motors, mechanical servo machines were created for forming applications, enabling complex deformation of sheet and bulk metal in the forming process [8–11]. Chen and Zhao *et al.* [12] proposed a high-capacity press system using two servo motors to drive a seven-bar linkage. The performance of the press was demonstrated, and kinematic experiments and metal forming experiments were carried out on the prototype press using a grating scale system. The resulting data matched the theoretical calculations well, which validates the feasibility of the new machine.

Instead of performing simple 1-stroke per stamping processes, the movements of rams in these machines are designed to change over time, allowing the use of one die for multiple operations and improving the mechanical properties of the material to prevent cracking or springback at the formed surfaces [13–15] (see Fig. 1). However, because flywheels are not employed and servo motor control requires high control feedback, these systems are only suitable for processing small parts and are too expensive for medium or small enterprises to buy. To overcome the use of servo motors, presses using complex stamping motion have been developed. Halicioglu and Assylbek *et al.* [16] proposed a single degree of freedom (1-DOF) eight-bar mechanical press capable of generating dwell motion without using servo motors. An optimization methodology using the Genetic Algorithm (GA) was employed to determine the optimal dimensions for achieving the desired motion of dwell. By comparing the position, velocity, and acceleration of the slider, the optimized dimensions for the mechanism can be determined, which reduces Manufacturing difficulty and improves the performance of the whole system. Based on the Stephenson II mechanism, Assylbek and Halicioglu *et al.* [17] developed a new press using a ternary link and unique connecting rods to increase the balancing for the slider. The experimental results are verified against the theoretical results, confirming that the proposed press has better characteristics than conventional press machines, owing to the distribution of forces and reaction to the frame.

Based on the structure of the servo press, this paper proposes using a single DOF mechanical press using gear transmission to control the complex movement of the ram. The kinematic analysis was also conducted to inspect the operation of every link in the mechanism. Several system configurations using different gear sets were studied to observe the result in one cycle of the press. The study presents three contributions, which are as follows: First, the new system provides a viable option for constructing multi-stroke presses for large-sized elastic products while taking advantage of the relaxation characteristics of the material. Second, employing a simple method for determining the kinematics of the mechanism enables obtaining the kinetic of the whole system easily. Third, since the complex ram movement can be performed with the use of isochronous motors, the proposed system allows the use of a flywheel, which reduces the required power, manufacturing difficulty, and product cost.

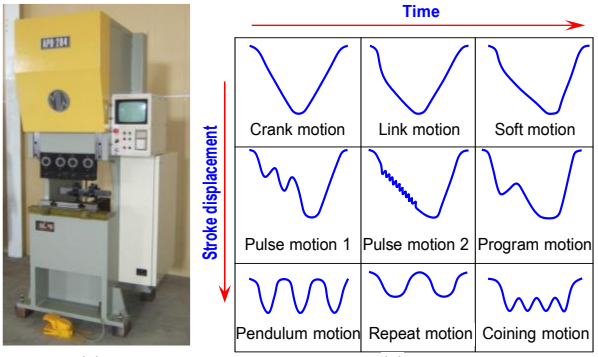

Figure 1. (a) Commercial servo stamping machines and (b) the ram's complex movements created by servo presses [13].

II. Kinematic Analysis

The proposed structure of the press consists of 6 links, as presented in Fig. 2.

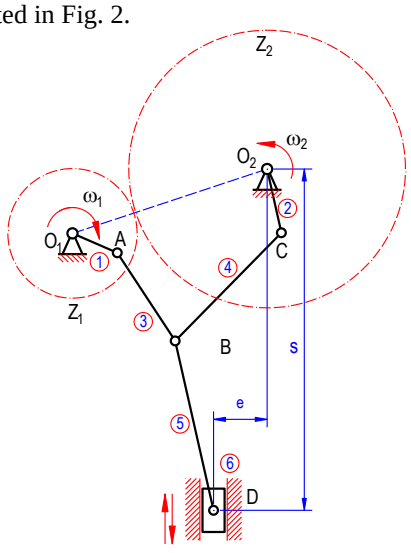

Figure 2. Structure of the proposed press.

By using a gear set Z_1-Z_2, the rotation of Link 1 is transmitted to Link 2 with a ratio $i=\omega_2/\omega_1=-Z_1/Z_2$. Since these links are directly connected to Links 3 and 4, the position of the connected joint B can be determined, and the movement of the ram head 6 is calculated. By replacing the gear set Z_1 and Z_2 with another set Z_3-Z_4 while maintaining the distance between O_1 and O_2, the rotation ω_2 of Link 2 can be changed, and allow the movement of slider 6 to be adjusted into different complex movements.

To determine the position of the component frames, vector loops are assigned to the mechanism, which can be divided into three closed loops separated by different colors, as presented in Fig. 3. By solving the position equation for each loop, the movement of the ram can be easily determined.

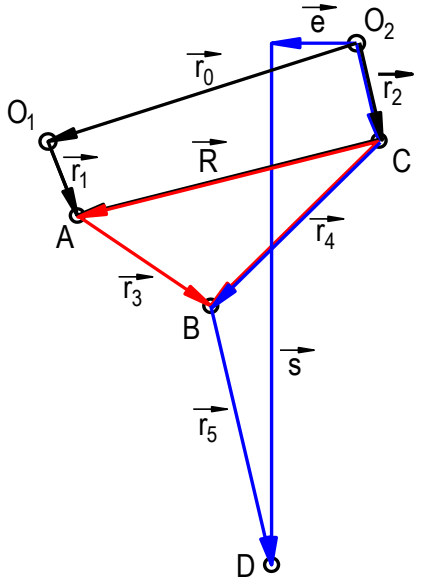

Figure 3. Dividing the mechanism into three separated loops.

As illustrated in Fig. 4, the first closed-loop equation includes four vectors:

$$\vec{r}_0+\vec{r}_1-\vec{r}_2=\vec{R} \tag{1}$$

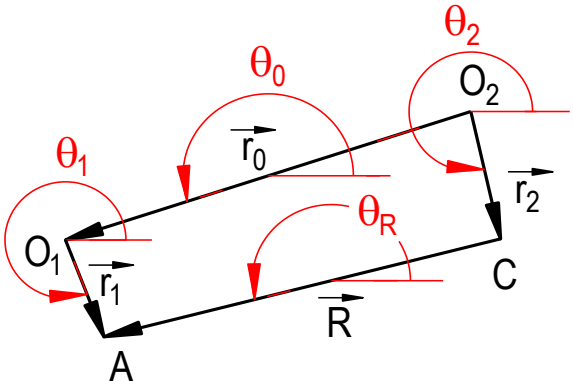

Figure 4. The first closed-loop vector equation.

This equation can be separated into scalar component equation in x- and y- directions, respectively, as:

$$\begin{cases} R\cos\theta_R = r_0\cos\theta_0 + r_1\cos\theta_1 - r_2\cos\theta_2 \\ R\sin\theta_R = r_0\sin\theta_0 + r_1\sin\theta_1 - r_2\sin\theta_2 \end{cases} \tag{2}$$

Draw R and θ_0 from the system Eq. (2):

$$\begin{cases} R = \sqrt{\left(R\cos\theta_R\right)^2 + \left(R\sin\theta_R\right)^2} \\ \theta_0 = \operatorname{atan}\left(\dfrac{R\cos\theta_R}{R\sin\theta_R}\right) \end{cases}$$

$$\rightarrow \begin{cases} R = \sqrt{\begin{aligned} &r_0^2 + r_1^2 + r_2^2 + 2r_0r_1\cos\left(\theta_0-\theta_1\right) - \\ &-2r_0r_2\cos\left(\theta_0-\theta_2\right) - 2r_1r_2\cos\left(\theta_1-\theta_2\right) \end{aligned}} \\ \theta_R = \operatorname{atan}\left(\dfrac{r_0\sin\theta_0 + r_1\sin\theta_1 - r_2\sin\theta_2}{r_0\cos\theta_0 + r_1\cos\theta_1 - r_2\cos\theta_2}\right) \end{cases} \tag{3}$$

The second loop contains three vectors (see Fig. 5), whose position can be determined by substituting the position of $\vec{R}$ (R and θ_0) into triangle ABC:

$$\delta_3 = \operatorname{acos}\left(\frac{R^2 + r_3^2 - r_4^2}{2Rr_3}\right) \tag{4}$$

$$\delta_4 = \operatorname{acos}\left(\frac{R^2 + r_4^2 - r_3^2}{2Rr_4}\right) \tag{5}$$

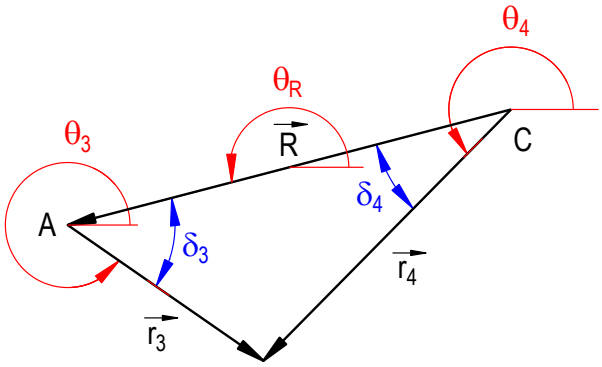

Figure 5. The second closed-loop vector.

And orientation angles of Links 3 and 4 can be obtained as:

$$\theta_3 = \theta_R + \pi - \delta_3 \tag{6}$$

$$\theta_4 = \theta_R + \delta_4 \tag{7}$$

As presented in Fig. 6, the third loop equation consists five components:

$$\vec{r}_2+\vec{r}_4+\vec{r}_5=\vec{e}+\vec{s} \tag{8}$$

Notice that $\vec{s}$ is the fixed-direction vector (the ram only oscillates vertically towards the anvil), and e represents the structural dimension (fixed distance). Resolving these component vectors into x- and y- directions:

$$\begin{cases} r_2\cos\theta_2+r_4\cos\theta_4+r_5\cos\theta_5=e\cos(-\pi)=-e \\ r_2\sin\theta_2+r_4\sin\theta_4+r_5\sin\theta_5=s\sin\left(\dfrac{-\pi}{2}\right)=-s \end{cases} \tag{9}$$

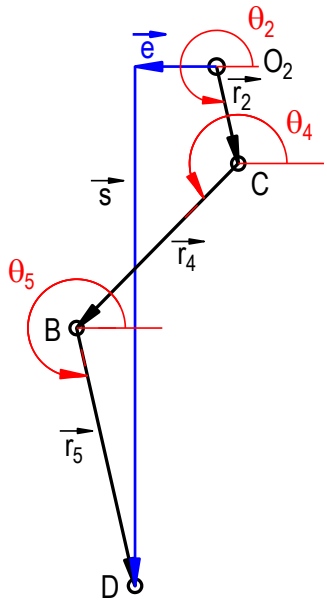

Figure 6. The third closed-loop vector equation.

Draw s from the system Eq. (9):

$$s=-\left(r_2\sin\theta_2+r_4\sin\theta_4+r_5\sin\theta_5\right) \tag{10}$$

Draw angular position of Link 5 from the system (9):

$$\theta_5=\text{acos}\left[\frac{-e-\left(r_2\cos\theta_2+r_4\cos\theta_4\right)}{r_5}\right] \tag{11}$$

With the transmission ratio between driver links $i=\dfrac{\omega_2}{\omega_1}=-\dfrac{Z_1}{Z_2}$, the corresponding rotational of Link 2 can be calculated:

$$\omega_2=\omega_1\times i \tag{12}$$

And the position of this link can be determined as:

$$\theta_2=\theta_1\times i+\Delta\varphi \tag{13}$$

where Δφ is the initial angle difference between these links.

The velocities and acceleration of the system can be obtained by deriving the equation of position closed loops. Since the positions of all links are obtained from the equations above, instead of using the closed loops in Figs. 4 and 5, a new loop is proposed for determining velocities and acceleration, as follows:

$$\vec{r_0}+\vec{r_1}+\vec{r_3}=\vec{r_2}+\vec{r_4} \tag{14}$$

Transform into Euler's formula:

$$r_0e^{j\theta_0}+r_1e^{j\theta_1}-r_2e^{j\theta_2}=r_4e^{j\theta_4}-r_3e^{j\theta_3} \tag{15}$$

Derivate Eq. (14) to obtain the velocity equation:

$$r_1j\omega_1e^{j\theta_1}-r_2j\omega_2e^{j\theta_2}=r_4j\omega_4e^{j\theta_4}-r_3j\omega_3e^{j\theta_3} \tag{16}$$

Divide both sides of the Eq. (16) for $je^{j\theta_3}$ and $je^{j\theta_4}$ to acquire new equations contain je^{j0° factor:

$$\begin{cases} r_1\omega_1e^{j(\theta_1-\theta_4)}-r_2\omega_2e^{j(\theta_2-\theta_4)}=r_4\omega_4e^{j0^\circ}-r_3\omega_3e^{j(\theta_3-\theta_4)} \\ r_1\omega_1e^{j(\theta_1-\theta_3)}-r_2\omega_2e^{j(\theta_2-\theta_3)}=r_4\omega_4e^{j(\theta_4-\theta_5)}-r_3\omega_3e^{j0^\circ} \end{cases} \tag{17}$$

Project the component equations into y-direction:

$$\begin{cases} r_1\omega_1\sin\left(\theta_1-\theta_4\right)-r_2\omega_2\sin\left(\theta_2-\theta_4\right)= \\ \qquad =-r_3\omega_3\sin\left(\theta_3-\theta_4\right)=r_3\omega_3\sin\left(\theta_4-\theta_3\right) \\ r_1\omega_1\sin\left(\theta_1-\theta_3\right)-r_2\omega_2\sin\left(\theta_2-\theta_3\right)= \\ \qquad =r_4\omega_4\sin\left(\theta_4-\theta_3\right) \end{cases}$$

Velocities of Link 3 and 4 hence can be drawn from the new system:

$$\begin{cases} \omega_4=\dfrac{r_1\omega_1\sin\left(\theta_1-\theta_3\right)-r_2\omega_2\sin\left(\theta_2-\theta_3\right)}{r_4\sin\left(\theta_4-\theta_3\right)} \\ \omega_3=\dfrac{r_1\omega_1\sin\left(\theta_1-\theta_4\right)-r_2\omega_2\sin\left(\theta_2-\theta_4\right)}{r_3\sin\left(\theta_4-\theta_3\right)} \end{cases} \tag{18}$$

Transform Eq. (8) into Euler's formula:

$$r_2e^{j\theta_2}+r_4e^{j\theta_4}+r_5e^{j\theta_5}=e.e^{-j\pi}+s.e^{-j\frac{\pi}{2}} \tag{19}$$

Derivating Eq. (18) to obtain velocity equation:

$$r_2\omega_2je^{j\theta_2}+r_4\omega_4je^{j\theta_4}+r_5\omega_5je^{j\theta_5}=\dot{s}.e^{-j\frac{\pi}{2}} \tag{20}$$

Divide both aside of the Eq. (20) for $je^{j\theta_5}$:

$$r_2\omega_2 e^{j(\theta_2-\theta_5)} + r_4\omega_4 e^{j(\theta_4-\theta_5)} + r_5\omega_5 e^{j0^\circ} = \\ = -\dot{s}je^{j\left(-\frac{\pi}{2}-\theta_5\right)} = -\dot{s}e^{-j\theta_5} \tag{21}$$

Projecting Eq. (20) into x- and Eq. (21) into y-directions:

$$\begin{cases} r_2\omega_2\cos\theta_2 + r_4\omega_4\cos\theta_4 + r_5\omega_5\cos\theta_5 = -\dot{s}\cos\left(-\frac{\pi}{2}\right) = 0 \\ r_2\omega_2\sin\left(\theta_2-\theta_5\right) + r_4\omega_4\sin\left(\theta_4-\theta_5\right) + r_5\omega_5\sin 0^\circ = -\dot{s}.\sin\theta_5 \end{cases} \tag{22}$$

The remaining velocities parameters are determined as:

$$\begin{cases} \omega_5 = -\dfrac{r_2\omega_2\sin\theta_2 + r_4\omega_4\sin\theta_4}{r_5\sin\theta_5} \\ \dot{s} = -\dfrac{r_2\omega_2\sin\left(\theta_2-\theta_5\right) + r_4\omega_4\sin\left(\theta_4-\theta_5\right)}{\sin\theta_5} \end{cases} \tag{23}$$

Notice that $\dfrac{e^{j\theta_m}}{e^{j\theta_n}} = e^{j(\theta_m-\theta_n)}$ and $je^{j\theta_k} = e^{j\left(\theta_k+\frac{\pi}{2}\right)}$, with θ_m, θ_n, θ_k respectively is the direction of links m, n, k. Continue derivating Eq. (16) of the linkage to acquire acceleration data:

$$r_1\omega_1^2 e^{j(\theta_1+\pi)} - r_2\omega_2^2 e^{j(\theta_2+\pi)} = r_4\omega_4^2 e^{j(\theta_4+\pi)} + \\ + r_4\varepsilon_4 e^{j\left(\theta_4+\frac{\pi}{2}\right)} - r_3\omega_3^2 e^{j(\theta_3+\pi)} - r_3\varepsilon_3 e^{j\left(\theta_3+\frac{\pi}{2}\right)} \tag{24}$$

Divide each side of Eq. (22) for $e^{j\theta_3}$ and $e^{j\theta_4}$, a new system is obtained:

$$\begin{cases} r_1\omega_1^2 e^{j\left(\theta_{14}+\frac{\pi}{2}\right)} - r_2\omega_2^2 e^{j\left(\theta_{24}+\frac{\pi}{2}\right)} = r_4\omega_4^2 e^{j\frac{\pi}{2}} + \\ \quad + r_4\varepsilon_4 e^{j0^\circ} - r_3\omega_3^2 e^{j\left(\theta_{34}+\frac{\pi}{2}\right)} - r_3\varepsilon_3 e^{j\theta_{34}} \\ r_1\omega_1^2 e^{j\left(\theta_{13}+\frac{\pi}{2}\right)} - r_2\omega_2^2 e^{j\left(\theta_{23}+\frac{\pi}{2}\right)} = r_4\omega_4^2 e^{j\left(\theta_{43}+\frac{\pi}{2}\right)} + \\ \quad + r_4\varepsilon_4 e^{j\theta_{43}} - r_3\omega_3^2 e^{j\frac{\pi}{2}} - r_3\varepsilon_3 e^{j0^\circ} \end{cases} \tag{25}$$

Projecting component equations of system Eq. (25) to the y-directions:

$$\begin{cases} r_1\omega_1^2\sin\left(\theta_{14}+\frac{\pi}{2}\right) - r_2\omega_2^2\sin\left(\theta_{24}+\frac{\pi}{2}\right) = \\ = r_4\omega_4^2\sin\frac{\pi}{2} - r_3\omega_3^2\sin\left(\theta_{34}+\frac{\pi}{2}\right) - r_3\varepsilon_3\sin\theta_{34} \\ r_1\omega_1^2\sin\left(\theta_{13}+\frac{\pi}{2}\right) - r_2\omega_2^2\sin\left(\theta_{23}+\frac{\pi}{2}\right) = \\ = r_4\omega_4^2\sin\left(\theta_{43}+\frac{\pi}{2}\right) + r_4\varepsilon_4\sin\theta_{43} - r_3\omega_3^2\sin\frac{\pi}{2} \end{cases} \tag{26}$$

$$\leftrightarrow \begin{cases} r_1\omega_1^2\cos\theta_{14} - r_2\omega_2^2\cos\theta_{24} = \\ = r_4\omega_4^2 - r_3\omega_3^2\cos\theta_{34} - r_3\varepsilon_3\sin\theta_{34} \\ r_1\omega_1^2\cos\theta_{13} - r_2\omega_2^2\cos\theta_{23} = \\ = r_4\omega_4^2\cos\theta_{43} + r_4\varepsilon_4\sin\theta_{43} - r_3\omega_3^2 \end{cases} \tag{27}$$

Draw acceleration of Link 3 and 4 from component Eq. (25):

$$\begin{cases} \varepsilon_3 = \dfrac{-r_1\omega_1^2\cos\theta_{14} + r_2\omega_2^2\cos\theta_{24} - r_3\omega_3^2\cos\theta_{34} + r_4\omega_4^2}{r_3\sin\theta_{34}} \\ \varepsilon_4 = \dfrac{r_1\omega_1^2\cos\theta_{13} - r_2\omega_2^2\cos\theta_{23} + r_3\omega_3^2 - r_4\omega_4^2\cos\theta_{43}}{r_4\sin\theta_{43}} \end{cases} \tag{28}$$

To obtain acceleration of the ram and Link 6, derivate the velocity Eq. (20):

$$r_2\omega_2^2 e^{j(\theta_2+\pi)} + r_4\omega_4^2 e^{j(\theta_4+\pi)} + r_4\varepsilon_4 e^{j\left(\theta_4+\frac{\pi}{2}\right)} + \\ + r_5\omega_5^2 e^{j(\theta_5+\pi)} + r_5\varepsilon_5 e^{j\left(\theta_5+\frac{\pi}{2}\right)} = \ddot{s}.e^{-j\frac{\pi}{2}} \tag{29}$$

Divide both side of Eq. (27) for $e^{j\left(\theta_5+\frac{\pi}{2}\right)}$:

$$r_2\omega_2^2 e^{j\left(\theta_{25}+\frac{\pi}{2}\right)} + r_4\omega_4^2 e^{j\left(\theta_{45}+\frac{\pi}{2}\right)} + r_4\varepsilon_4 e^{j\theta_{45}} + \\ + r_5\omega_5^2 e^{j\frac{\pi}{2}} + r_5\varepsilon_5 e^{j0^\circ} = \ddot{s}.e^{-j(\theta_5+\pi)} \tag{30}$$

Projecting Eq. (20) into x- and Eq. (21) into y-directions:

$$\begin{cases} r_2\omega_2^2\cos\theta_2 + r_4\omega_4^2\cos\theta_4 + r_4\varepsilon_4\sin\theta_4 + r_5\omega_5^2\cos\theta_5 + r_5\varepsilon_5\sin\theta_5 = 0 \\ r_2\omega_2^2\cos\theta_{25} + r_4\omega_4^2\cos\theta_{45} + r_4\varepsilon_4\sin\theta_{45} + r_5\omega_5^2 = \ddot{s}\sin\theta_5 \end{cases} \tag{31}$$

Draw acceleration coefficients from the system:

$$\begin{cases} \varepsilon_5 = -\dfrac{r_2\omega_2^2\cos\theta_2 + r_4\omega_4^2\cos\theta_4 + r_4\varepsilon_4\sin\theta_4 + r_5\omega_5^2\cos\theta_5}{r_5\sin\theta_5} \\ \ddot{s} = \dfrac{r_2\omega_2^2\cos\theta_{25} + r_4\omega_4^2\cos\theta_{45} + r_4\varepsilon_4\sin\theta_{45} + r_5\omega_5^2}{\sin\theta_5} \end{cases} \tag{32}$$

III. Example and Discussion

Based on the system's movement concept, a 3D model of the system with the given component link lengths is constructed, as presented in Fig. 7.

One external mated gear train with a ratio $i = -Z_1/Z_2 < 0$ is assembled in the driving shafts, making them to rotate in different directions. The angular difference $\Delta\varphi$ between these shafts is adjusted by aligning the position of point B in the circular grove of the gear attached to shaft 2. If gear 1 is removed and gear 2 is fixed, the gear ratio $i = 0$ and

the system becomes a knuckle joint press, with the position of point B still adjustable (to give different values for Δφ). By simply changing the position of gears Z_1 and Z_2 with two driving links, a new transmission ratio $i' = -Z_2/Z_1$ can be created, which also improves the flexibility of the system in constructing the movement of the ram head. Through the movement of driving links, links 3 and 4 move, forming a closed chain, providing a defined locus for revolution joint B. Through displacement of point B, connecting rod 5 transmits motion to ram head 6, creating complex oscillating movement.

In the proposed configuration, a gear set with gear ratio $i = -0.5$ was employed, and driving speed for link 1 is pre-assigned as ω_1=60 rpm. The initial angular difference Δφ between links 1 and 2 was randomly selected to survey the ability to change the functional movement of the ram head. By changing the gear mating orientation (to obtained different ratio $i = -0.5$, -2.0, and 0) and adjusting the angular difference a, three graphs, including the movement of the ram, are illustrated, as presented in Fig. 8. The total stroke of each ratio was also calculated to determine the case that has the required stroke for the stamping process.

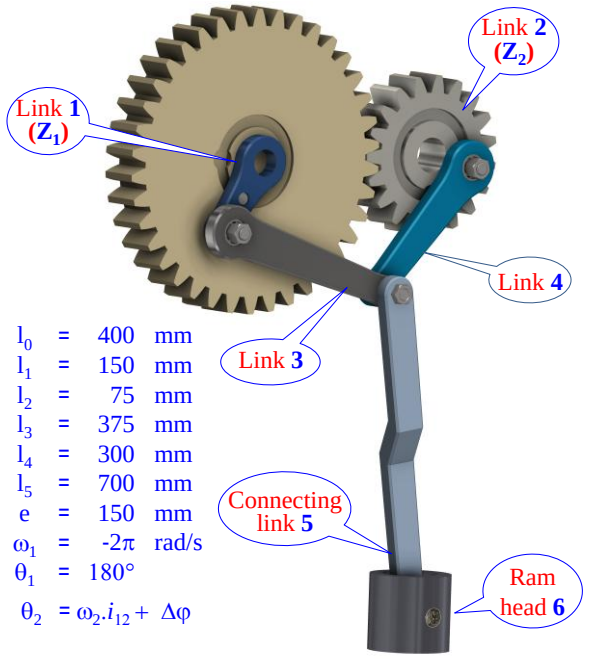

Figure 7. Structure of the proposed system.

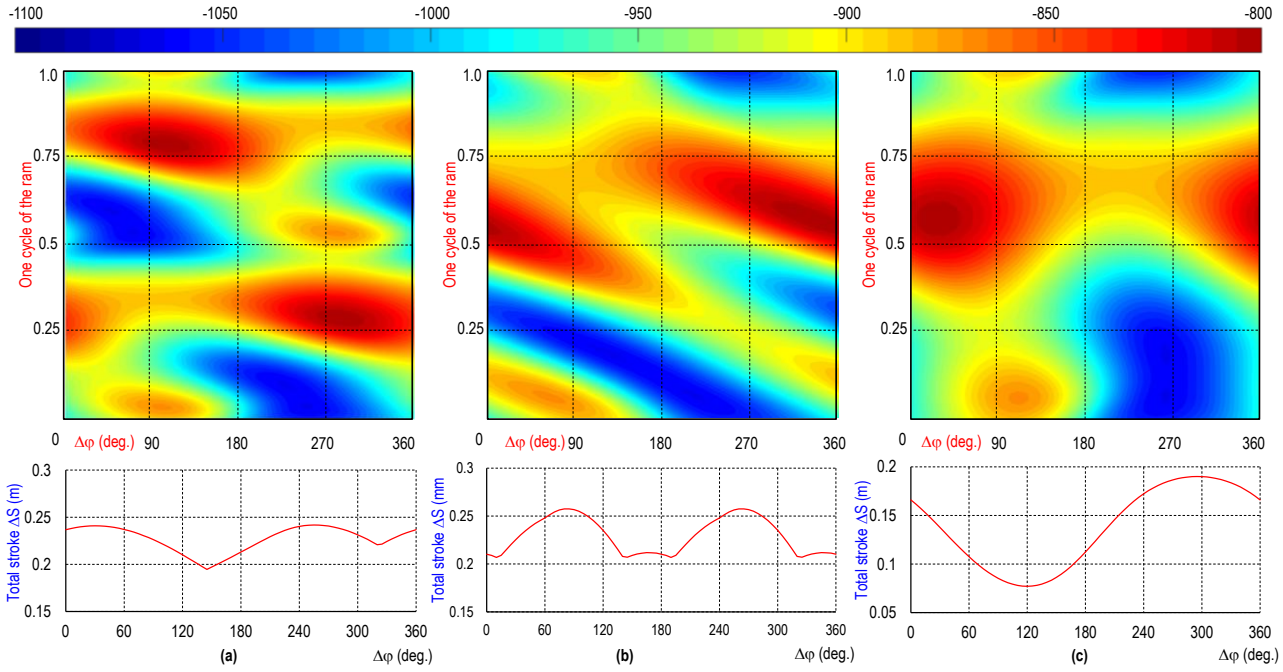

Figure 8. Ram's movement in one cycle and the maximum stroke corresponding to different value of Δφ with the gear set ratio: (a) i=–0.5; (b) i=–2.0, and (c) i=0 (unit: mm).

For a detailed analysis, six different ram movements were extracted from the graphs and presented in Fig. 9. With the gear ratio $i = -0.5$, Link 3 is driven with a rotational speed of 30 rpm and creates 2-second cycle stamping processes. If the initial angular difference Δφ between the links is 290 °(in Case 1), the ram will operate with three stroke displacements are 0.11, 0.18, and 0.25 m, respectively. If the angular difference Δφ=120 °(in Case 2), the ram can perform another movement with respectively stroke displacements are 0.12, 0.20, and 0.22 m. By reversing the assembly of gear Z_1 and Z_2 to obtain a ratio of $i = -2.0$, other 1-second stamping processes with different ram displacements were created, as presented in Cases 3 and 4. If gear 2 is detached (i = 0), dwell or coining movements of the ram can be acquired just by adjusting the angular difference Δφ (Cases 5 and 6), with each cycle lasting one second.

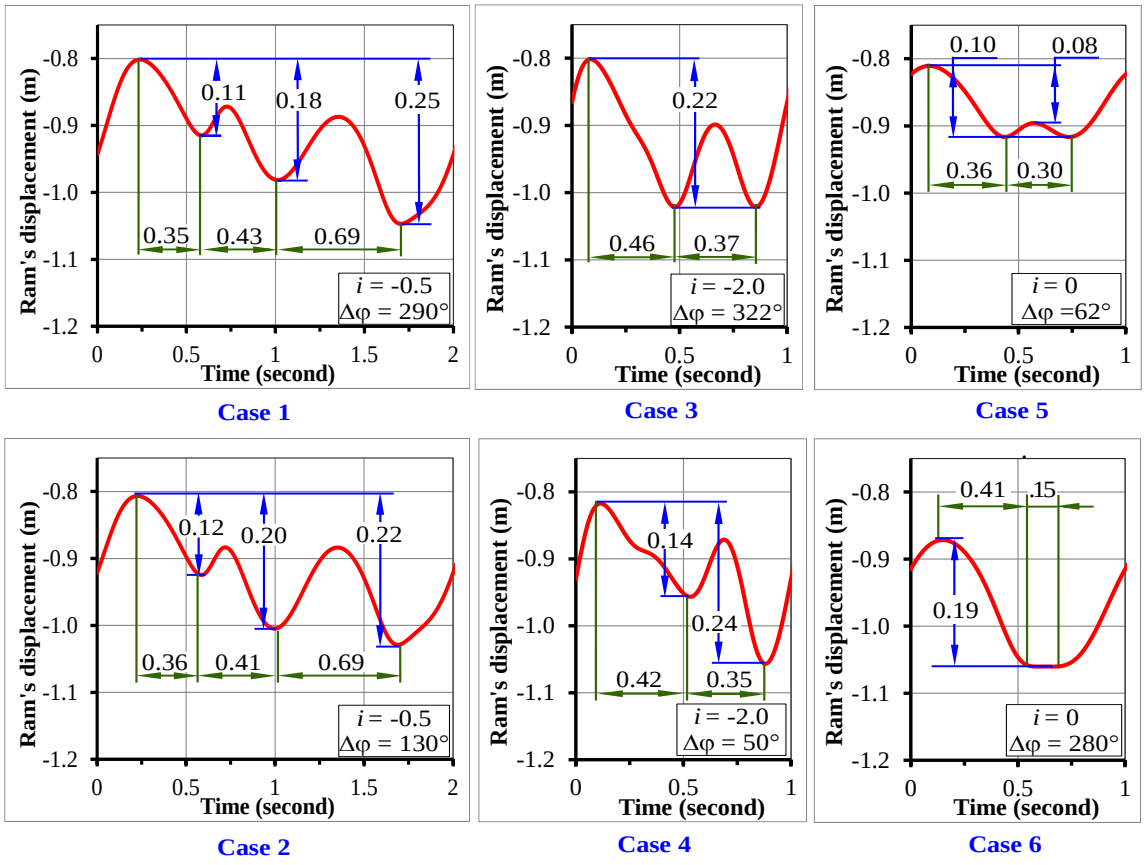

Figure 9. Different ram movements obtained by adjusting initial parameters (i and Δφ) of the driving links.

In analyzing the stamping process, determining the dynamic stroke of the ram is the most important aspect. Hence only the movement of the ram is analyzed, and the evaluation of velocities and accelerations of Links 3-4-5 is ignored. By substituting the configurations dimensions from Fig. 8 with different gear ratios into Eq. (23) and Eq. (32); the corresponding velocity and acceleration of the ram can be obtained and summarized in Figs. 10 and 11.

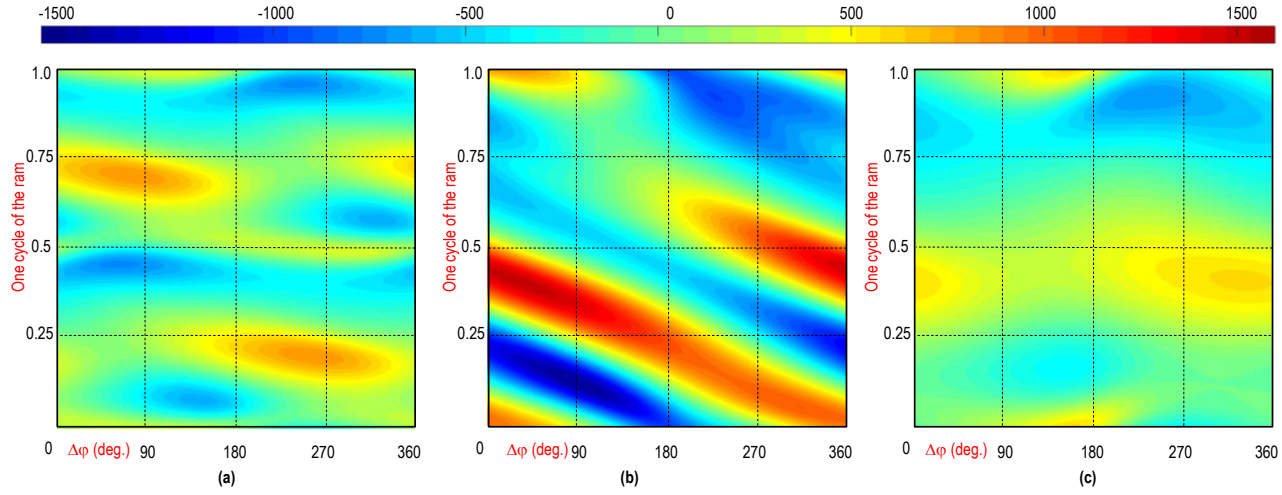

Figure 10. Velocity of ram in one cycle corresponding to different value of Δφ with the gear set ratio:(a) i=–0.5; (b) i=–2.0, and (c) i=0 (unit: mm/s).

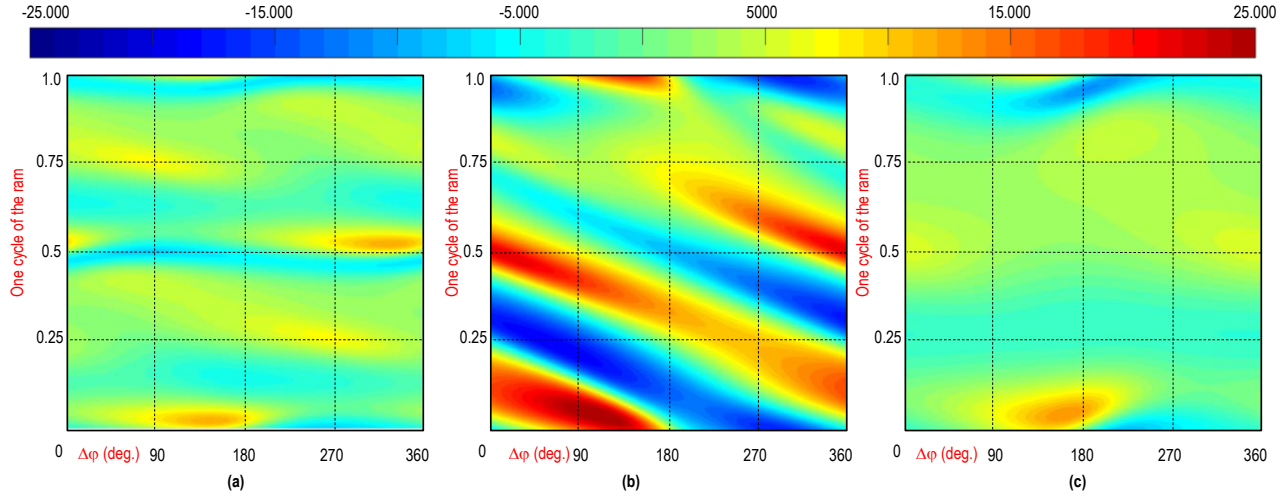

Figure 11. Acceleration of ram in one cycle corresponding to different value of Δφ with the gear set ratio: (a) i=–0.5; (b) i=–2.0, and (c) i=0 (unit: mm/s^2).

The resulting graphs show that when absolute value of the gear ratio I is less than 1 ($|i|$<1), link 3 rotates at a slower speed, resulting in a longer cycle duration compared to those with $|i|$>1 and i=0 (which have a cycle duration of 1 second). In the case $|i|$>1, where link 2 overdrive speed of link 1, the velocity and acceleration of component links, especially in the ram, are much higher than in other cases. It can be seen from Fig. 11 that while the maximum velocity and acceleration of the ram are only 10^3 mm/s and 10^4 mm/s^2 for ratios i=−0.5 or i=0, those values are more than 1,600 m/s and up to 2.3×10^4 mm/s^2 for ratio i=−2. This can be explained by the fact that the speed of link 2 has a direct influence on the movement of the ram, making it move with higher intensity compared to others ratios.

The above graphs also provide data for arbitrary values of the initial angular difference (Δφ) for detailed analysis. For example, the velocity and acceleration of the six cases from Fig. 9 can be calculated and presented in Fig. 12. Even with 3-stage stamping movement of the ram (Cases 1 and 2), because the gear ratios used are $|i|$=0.5 < 1, their velocity and acceleration are much smaller than those in Cases 3 and 4, which have ratios of $|i|$ =2 > 1.

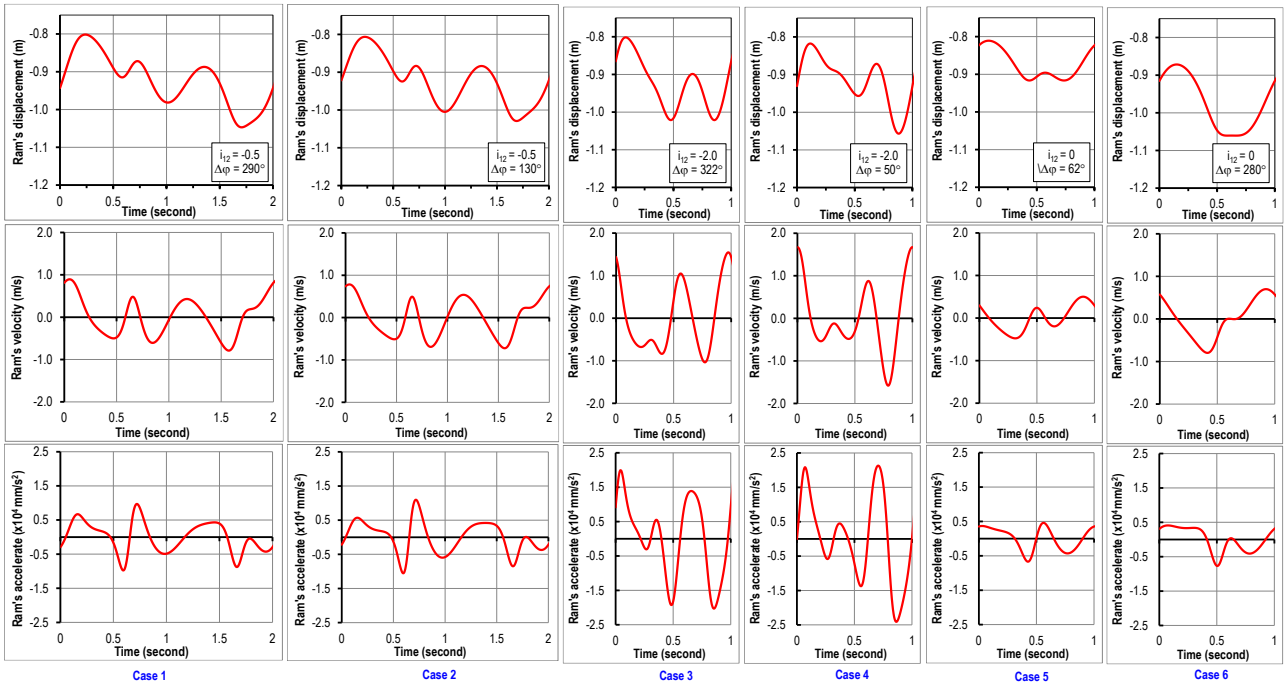

Figure 12. Velocities and accelerations of the ram for six configurations from Figure 7.

Compared to the motion in Fig. 1, it can be observed that even with an isochronous motor, the proposed system can produce ram movements similar to those of complex stamping from servo stamping presses. As the stroke of the

ram can be adjusted before each process (replacing gears with different ratios or aligning the angular difference between driving shafts), the proposed system does not require servo motors and can utilize flywheels to increase energy storage capacity for heavy duties, regardless of the complexity of the ram's movements. Furthermore, because it does not necessitate the adjustment of the component links' length, this structure is more stable and rigid. These characteristics can reduce construction costs and machine size, improving the press's efficiency and power. Additionally, the ram stroke, ranging from 75 to 260 mm, is another strong point of the system, not only allowing for the stamping of thin plates but also enabling the expansion of forging complex-shaped objects without replacing dies.

IV. Conclusion

This research proposes a new structure for press machines that can perform complex movements. By adjusting initial parameters for the gear transmission, some multi-stroke cycles of the ram are obtained, proving the applicability of the proposed system in the multi-stage forging process. The main conclusion and achievements of this study are drawn as follows:

With the use of a gear train into the six-bar linkage, which allow change the driving ratios and adjust the angular difference between driving link, the new mechanism can be perform complex movements, which are benefit for metal forming while utilized the relaxation of material.

By solving simple kinematic equations of component frame's length, the movement of the slider can be synthesis and summarized. From the obtain results, the requirement combination (i, $\Delta\varphi$) of the structure can be determined according to the press specifications and forming requirement.

Since the proposed system only uses isochronous motors, its construction is much simpler than systems that require servo motors to achieve complex stamping processes. Furthermore, since the ram movement is predetermined, there is no need for a feedback circuit to control it. Thus, the new system can incorporate flywheels to store energy and decrease the required motor power, leading to enhanced manufacturing efficiency and reduced product costs.

Conflict of Interest

The authors declare no conflict of interest.

Author Contributions

N. D. N. conducted and supervised the research; D. A. T. analyzed the data; D. A. T wrote the manuscript; All authors had approved the final version.

Acknowledgment

A special thanks to the Thai Nguyen University of Technology for funding this research.

References

[1] K. Hariharan, O. Majidi, C. Kim, M. G. Lee, F. Barlat, "Stress relaxation and its effect on tensile deformation of steels," *Materials & Design (1980–2015)*, vol. 52, pp. 284–288, 2013.

[2] A. Mukasheva, S. Japayev, G. Abdraimova, B. Kyrykbaev, K. Kozhamberdiyev, B. Uskembayeva, and A. Zhauyt, "A dynamic analysis of six-bar mechanical press," *Vibroengineering Procedia*, vol. 13, pp. 249–254, 2017.

[3] W. H. Hsieh and C. H. Tsai, "On a novel press system with six links for precision deep drawing," *Mechanism and Machine Theory*, vol. 4, no. 2, pp. 239–252, 2011.

[4] A. Tuleshov, B. Akhmetova, and B. Merkibayeva, "Analytical synthesis and study of the functional capabilities of the stephenson II mechanism for crank presses," *International Journal of Mechanical Engineering and Robotics Research*, vol. 11, no. 11, pp. 850–857, 2022.

[5] S. Mitsi, I. Tsiafis, and K. D. Bouzakis, "Dynamic analysis of six-bar mechanical press for deep drawing,". *IOP Conf. Ser.: Mater. Sci. Eng.*, 2017, vol. 174, 012006.

[6] M. S. Jo, J. K. Shim, H. S. Park, and W. R. Kim, "Dimensional synthesis of watt II and stephenson III six-bar slider-crank function generators for nine prescribed positions," *Applied Sciences*, vol. 12, no. 20, 10503, 2022.

[7] R. C. Soong, "A new design method for single DOF mechanical presses with variable speeds and length-adjustable driving links," *Mechanism and Machine Theory*, vol. 45, no. 3, pp. 496–510, 2010.

[8] H. Ando, "Application of servo system in recent press machines," *Journal of the Japan Society for Technology of Plasticity*, vol. 45, no. 526, pp. 877–882, 2004. (in Japanese).

[9] T. Altan and A. Groseclose, "Servo-drive presses-recent developments," ERC/NSM and CPF-Ohio State University, 2009.

[10] Japan Machinery Federation, Japan Forming Machinery Association, *Standardization of Servo-Motor Drive Press Machines*, 2005. (in Japanese).

[11] W. Z. Guo, K. He, K. Yeung, and R. Du, "A new type of controllable mechanical press: motion control and experiment validation," *Journal of Manufacturing Science and Engineering*, vol. 127, no. 4, pp. 731–742, 2005.

[12] L. Chen, S. D. Zhao, and J. X. Li, "Design and analysis of a novel seven-bar mechanical servo press with dual motors inputs," in *Proc. the Institution of Mechanical Engineers, Part C: Journal of Mechanical Engineering Science*, vol. 231, no. 20, 2017, pp 3855–3865.

[13] K. Osakada, K. Mori, T. Altan, and P. Groche, "Mechanical servo press technology for metal forming," *CIRP annals*, vol. 60, no. 2, pp. 651–672, 2011.

[14] C. C. Kuo, H. L. Huang, T. C. Li, K. L. Fang, and B. T. Lin, "Optimization of the pulsating curve for servo stamping of rectangular cup," *Journal of Manufacturing Processes*, vol. 56, pp. 990–1000, Aug 2020.

[15] T. C. Chen, S. X. Chen, C. C. Wang, and T. E. Lee, "Analysis of the punch motion curve for the springback of U-shaped sheet metal," *Advances in Mechanical Engineering*, vol.15, no. 3, 2023. doi:10.1177/16878132231161151

[16] R. Halicioglu, J. Assylbek, and K. Moldir, "Optimum design and analysis of a novel planar eight-bar linkage mechanism," *Mechanics Based Design of Structures and Machines*, pp. 1–22, 2021. doi: 10.1080/15397734.2021.1995410

[17] J. Assylbek, R. Halicioglu, and K. Moldir, "Kinetostatic analysis, manufacturing, and experimental application of a press machine based on Stephenson II mechanism," in *Proc. the Institution of Mechanical Engineers, Part B: Journal of Engineering Manufacture*, vol. 236, no. 8, 2022, pp. 1113–1124.